國立雲林科技大學
98學年度博士班招生考試試題

所別：化學工程與材料工程系
科目：科技文獻

根據附件一，回答下列問題：

1. 請以中文製作本文獻的摘要 (10%)

2. 根據本文獻，以 chemical hydrides 方式儲氫時有哪些問題應予重視？ (20%)

3. 根據本文獻，以 chemical hydrides 方式儲氫有何優勢與缺點？ (20%)

根據附件二，回答以下問題：

4. 【20% 】本文所討論的導電性高分子 Polypyrrole 和 BTEX 之間的關係爲何？連結該關係的科學基礎爲何？

5. 【20% 】本文中，IGC 和導電性高分子 Polypyrrole 之表面自由能之間的關係爲何？連結該關係的科學基礎爲何？

6. 【10% 】 圖 11 所顯示的數據（含 C6~C9，benzene, toluene, ethylbenzene, and *o-*, *m-*, *p-* xylene）和表面自由能之間的關係爲何？

Available online at www.sciencedirect.com
ScienceDirect
ELSEVIER
International Journal of Hydrogen Energy 33 (2008) 360–365
International Journal of HYDROGEN ENERGY
www.elsevier.com/locate/ijhydene

附件一

Chemical hydrides: A solution to high capacity hydrogen storage and supply

Rajesh B. Biniwale[a,*], S. Rayalu[a], S. Devotta[a], M. Ichikawa[b]

[a]National Environmental Engineering Research Institute, Nehru Marg, Nagpur 440020, India
[b]Catalysis Research Center, Hokkaido University, Sapporo, Japan

Received 19 June 2007; accepted 9 July 2007
Available online 12 September 2007

Abstract

Cycloalkanes are good candidate media for hydrogen storage (6.5 wt% and 60–62 kg H_2/m^3). A novel approach for the supply of hydrogen, through liqaid organic hydrides (LOH) using catalytic reaction pair of dehydrogenation of cycloalkanes and hydrogenation of corresponding aromatics is a useful process for supply of hydrogen. Hydrogenation of aromatics is relatively well-established process. However, the efforts are needed to develop efficient catalyst for dehydrogenation of cycloalkanes. In this paper we review the dehydrogenation of cycloalkanes as useful reaction for storage of hydrogen in chemieal hydrides.

Keywords: Hydrogen storage; Liquid organic hydrides; Delivery to fuelling station; Cycloalkanes

1. Introduction

Onboard storage and supply of hydrogen for fuel cell is an important issue in the successful application of PEMFC. Also the transportation of H_2 from production facilities to the fuelling station needs to be considered for successful application of hydrogen economy [1,2]. Hydrogen being very flammable gas its transport involves several safety issues. The safety issues are related to the lower and higher explosion limits for H_2 concentration in air, low ignition energy in air and requirement of high pressure (typically 300–500 psi) storage or some times cryogenic temperatures, if it is transported in liquid form. These problems can be overcome if the hydrogen is either adsorbed on some materials such as carbon nano-tubes or chemically stabilized such as in the case of metal hydrides or alanates. Several studies report the development of hydrogen storage materials such as metal hydrides [3–6], Mg-based alloys [7,8], carbon materials [9–16], boron compounds [17], chemical hydrides [18], etc. While developing such hydrogen storage materials, capacity of the material in terms of weight and volume basis is an important factor to be considered. With a limited capacity it would result in weight penalty and CO_2 emissions associated with transportation. Also the adsorption and desorption kinetics is to be sufficiently fast to provide continuous H_2 supply. Another important requisite is to transport the hydrogen containing media at close to atmospheric temperature and pressure conditions and possibly using the existing infrastructure such as lorries.

Hydrogen containing chemicals which are useful for storage of hydrogen include methanol, ammonia and cycloalkanes. At STP all these are in liquid phase and therefore provide advantage of possibility of using existing infrastructure being used for gasoline. The hydrogen storage capacities of these chemical hydrides may range in the scale of 6–8 wt%. Earlier it was thought that since the chemical storage method is non-reversible, the compounds cannot be used in cycles. In view of this supply of hydrogen through liquid organic hydrides (LOH) using catalytic reaction pair of dehydrogenation of cycloalkanes such as methylcyclohexane, cyclohexane and decalin; and hydrogenation of corresponding aromatics is a useful process for supply of hydrogen to PEMFC. This is one of the most promising methods to store, transport and supply with in situ generation of hydrogen due to several advantages associated with this system which include; CO_x free hydrogen at fuelling stations, reversible catalytic reactions, recyclable reactants and products and relatively high hydrogen contents (6–8% on weight basis and about 60–62 kg H_2/m^3 on volume basis). Particularly,

* Corresponding author. Tel.: +91 9822745768.
E-mail address: rb_biniwale@neeri.res.in (R.B. Biniwale).

0360-3199/$ - see front matter © 2007 International Association for Hydrogen Energy. Published by Elsevier Ltd. All rights reserved.
doi:10.1016/j.ijhydene.2007.07.028

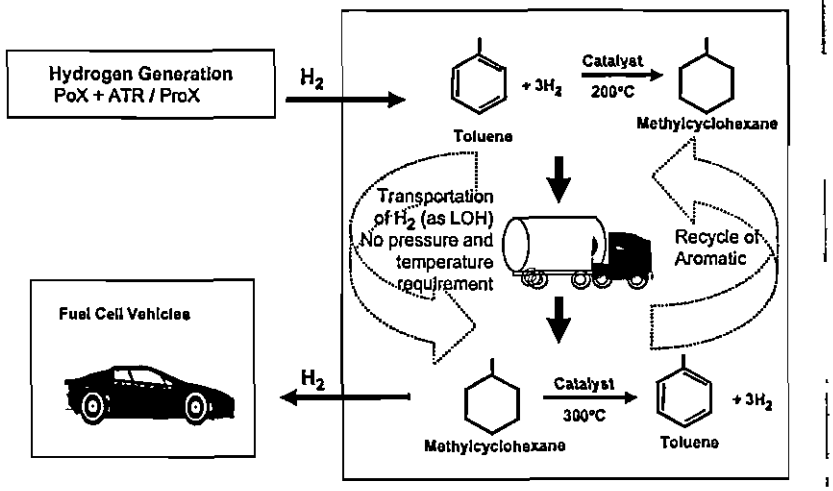

Fig. 1. Schematic of hydrogen storage and supply system.

the approach is most useful to transport the hydrogen from centralized generation facilities to fuelling stations. A schematic of catalytic reaction pair of hydrogenation of toluene and dehydrogenation of methylcyclohexane for hydrogen storage and supply is depicted in Fig. 1. Several studies have been reported on cycloalkanes as carrier for hydrogen and particularly development of dehydrogenation catalysts. The important issues being addressed by these reports are dehydrogenation temperature, dehydrogenation rates for various cycloalkanes, hydrogen evolution rates and reactor type for efficient heat transfer. Considering the development in this important field addressing hydrogen storage which is of current interest, this paper was envisaged to review state-of-art and to identify the future scope of research.

2. Cycloalkanes for hydrogen storage

Several cycloalkanes may be used as hydrogen carrier as LOH include cyclohexane, methylcyclohexane, teralin, decalin, cyclohexylbenzene, bicyclohexyl, 1-methyldecalin, etc. A few reactions of dehydrogenation of cycloalkanes are depicted in Fig. 2. One mole of cycloalkane has potential to transport 3–6 mol of hydrogen. The endothermic energy requirement for these reactions is in the range of 64–69 kJ per mole of H_2 this is much lower than energy that could be obtained by oxidation of H_2, 248 kJ/mol. Hydrogen storage capacities of cycloalkanes and other storage media are compared in the Table 1 along with boiling and melting points. Due to high boiling points of cycloalkanes, the present infrastructure such as oil tankers and tank lorries can be used for the long-term storage and long-distance transportation of hydrogen in the form of LOH.

3. Catalysts for dehydrogenation of cycloalkanes

Noble metal catalysts particularly Pt and bimetallic catalysts Pt–M (M = second metal) are well reported for highly selective dehydrogenation of cycloalkanes. Dehydrogenation of

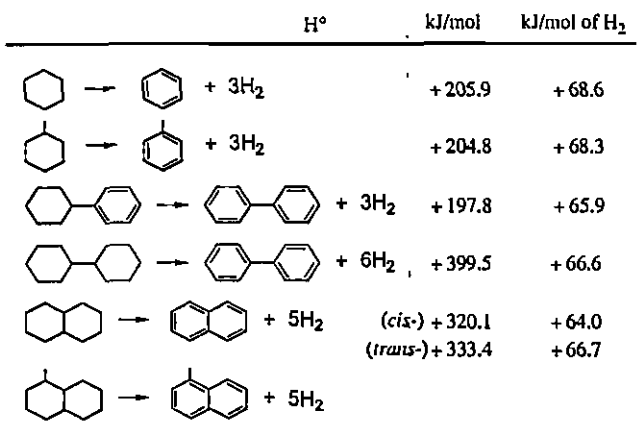

Fig. 2. Various potential cycloalkanes with hydrogen storage capacity and endothermic energy requirement.

Table 1
Hydrogen storage capacity of various media and their physical properties

Storage media	Hydrogen content		Boling point (°C)	Melting point (°C)
	wt%	mol/L		
Cyclohexane	7.2	27.77	80.7	6.5
Methylcyclohexane	6.2	23.29	101	−126.6
Tetralin	3.0	14.72	207	−35.8
cis-decalin	7.3	32.44	193	−43.0
trans-Decalin	7.3	31.46	185	−30.4
cyclohexylbenzene	3.8	17.63	237	4
bicyclohexyl	7.3	32.0	227	3
cis-syn-1-methyldecalin	6.6	29.31	213.2	−68
trans-anti-1-methyldecalin	6.6	28.52	204.9	−68
$LiH + H_2O$	7.8	4.1	–	680
$LiBH_4 + 4H_2O$	8.6	2.4	–	268
$LaNi_5H_6$	1.4	6.2	–	–
$MmNi_{4.5}Al_{0.25}Co_{0.25}H_{3.4}$	1.2	4.8	–	–
Liquid H_2 (with tank)	100 (5.11)	–	−252.9	–

methylcyclohexane over a Pt–Re/alumina catalyst in the presence of added hydrogen has been reported [19]. Pt and Pt–Re catalyst has been reported for dehydrogenation of methylcyclohexane to produce hydrogen [20]. Dehydrogenation of methylcyclohexane was reported by Newson et al. [21], Taube and Taube [22], Klvana et al. [23] and Grünenfelder and Schucan [24] for seasonal storage of energy through storage and supply of hydrogen using Pt-based catalysts. Various supports used for Pt catalysts include alumina, activated carbon and anodized aluminum. Catalytic decalin dehydrogeno-aromatization for long-term storage and long-distance transportation of hydrogen using catalyst Pt/C, Pt–Ir/C and Pt–W/C [25,26]. The addition of second metals such as Mo, W, Re, Rh, Ir and Pd on the carbon-supported Pt catalysts reported to result in enhanced dehydrogenation rate due to the promotion of C–H bond cleavage and/or desorption of aromatic products. A physical mixture of Pt/AC and Pd/AC catalysts exhibits higher activities than the monometallic Pt/AC catalyst owing to the synergistic effects of spillover, migration, and recombination of hydrogen over Pt and Pd catalysts [27]. In an attempt of designing catalysts using less Pt or non-noble metal catalysts Ni-based catalysts have been reported. These include Ni/C, Ru/C and Ni–Ru [28] and Ni–Pt catalysts for dehydrogenation reactions. Particularly Ni–Pt/AC catalysts has shown highly selective dehydrogenation of cyclohexane with minimum use of Pt. Selectivity towards hydrogenolysis was observed to be only 0.8–1.2% with addition of 0.5 wt% Pt in 20 wt% Ni [29]. Dehydrogenation of methylcyclohexane has been reported on K–Pt/Al_2O_3 catalyst at relatively higher temperature of 320 °C [30]. It appears from the literature available that the most active and selective catalyst for dehydrogenation of cycloalkanes is Pt. However, the bimetallic catalysts containing a small amount of Pt have promising potential for cost-effective catalysts.

The dehydrogenation is not a shape selective reaction and it is reported that when well-dispersed metal is present as catalyst then is the prevailing reaction as compared to hydrogenolysis. Activated carbon with high surface area is good support for well-dispersed metal catalysts. Further, absence of any acid sites on carbon support prevent cleavage of C–H bonds thus reduces the formation of carbon and in turn improves catalyst stability.

4. Comparison of various dehydrogenation catalysts

Hydrogen evolution rates reported over various catalysts under different reaction conditions and temperature are compared in Table 2. Most of the catalysts reported are Pt-based catalysts and reactions are carried out at temperatures ranging from 210–350 °C. Activated carbon in granule and cloth form, alumina and alumite are the supports used for catalysts. The most

Table 2
Hydrogen evolution rates reported for various cycloalkanes over different catalysts

Reactant	Catalysts	Temp. (°C)	H_2 evolution rate (mmol/g_{metal}/min)	Reactor system	Ref.
Cyclohexane	5 wt% Pt/AC	82	0.034	Batch-wise	[31]
Cyclohexane	3.82 wt% Pt/AC	300	1800	Batch-wise	Cross-ref of [32]
Cyclohexane	2 wt% Pt/Alumina	300	910	Batch-wise	Cross-ref of [32]
Methylcyclohexane	3.82 wt% Pt/AC	300	1700	Batch-wise	Cross-ref of [32]
Decalin	3.82 wt% Pt/AC	300	610	Batch-wise	Cross-ref of [32]
Cyclohexane	2 wt% Pt/Alumina	315	29	Flow-system	[27]
Cyclohexane	10 wt% Pt/AC cloth	260	98	Flow-system	[32]
Cyclohexane	10 wt% Pt/AC cloth	330	510	Flow-system	[32]
Methylcyclohexane	10 wt% Pt/AC cloth	298	520	Flow-system	[32]
Decalin	10 wt% Pt/AC cloth	320	460	Flow-system	[32]
Cyclohexane	Pt/alumite (Pt3 g/m^3)	300	1600	Flow-system	[32]
Cyclohexane	Pt/alumite (Pt3 g/m^3)	350	3800	Flow-system	[32]
Cyclohexane	12 wt% Pt–Rh/AC cloth	331	520	Flow-system	[32]
Cyclohexane	11 wt% Pt–Re/AC cloth	328	550	Flow-system	[32]
Cyclohexane	5 wt% Pt/AC	235	98	Spray-pulsed system	[29]
Cyclohexane	10 wt% Ni/AC	300	7.1	Spray-pulsed system	[29]
Cyclohexane	20 wt% Ni/AC	300	8.5	Spray-pulsed system	[29]
Cyclohexane	40 wt% Ni/AC	300	6.8	Spray-pulsed system	[29]
Cyclohexane	20 wt% Ni+0.5 wt% Pt/AC	300	13.1	Spray-pulsed system	[29]
Tetralin	5 wt% Pt/AC	210	103	Superheated liquid film	[28]
Tetralin	5 wt% Pt/AC	240	250	Superheated liquid film	[28]
Decalin	5 wt% Pt/C	210	12.35	Liquid film	[25]
Decalin	Pt–W/C (5 wt% metal)	210	42.31	Liquid film	
Decalin	Pt–Ir/C (5 wt% metal)	210	25.2	Liquid film	[25]
Tetralin	Pt–Ir/C (5 wt% metal)	210	19.6	Liquid film	[25]
Decalin	5 wt% Pt/C	210	55.5	Liquid film	[25]
Decalin	5 wt% Pt/C	210	83.3	Liquid film	[25]
Decalin	5 wt% Pt/C	210	160	Liquid film	[25]
Decalin	5 wt% Pt/C	210	444.4	Liquid film	[25]
Methylcyclohexane	0.1 wt% K+0.6 wt% Pt/Al_2O_3	320	744 (mmol/L_{cat}/min)	Fixed bed	[30]

active dehydrogenation system reported is in flow system under spray-pulsed injection of cyclohexane over Pt/alumite catalysts with hydrogen evolution rate of 3800 mmol/g/min. Whereas, in batch mode hydrogen evolution rate of 1800 mmol/g/min is reported for 3.82 wt% Pt/ AC at 300 °C. Under the spray-pulsed continuous reactor system again Pt/AC is having enhanced hydrogen evolution rate of 98 mmol/g/min as compared to Ni/AC catalysts. However, from the economic point of view it would be advantageous to use Ni-based catalysts. Reaction of decalin under the liquid film condition over 5 wt% Pt/C has exhibited hydrogen evolution rate of 444 mmol/g/min which is relatively high at temperature of 210 °C. When Pt–Ir/C (Pt/Ir = 4) or Pt–W/C (Pt/W = 1) catalysts were used under the same liquid film conditions it has shown hydrogen evolution of 25.2 and 42.31 mmol/g/min at 210 °C [25]. More recently considering higher rate of dehydrogenation, tetralin was used as hydrogen storage medium and dehydrogenation was carried out over 5 wt% Pt/C under superheated liquid film condition with hydrogen evolution rates of 103 and 250 mmol/g/min at 210 and 240 °C, respectively [28]. Another recent publication on K–Pt/Al_2O_3 catalyst has reported hydrogen evolution rate of 744 mmol/ min /L_{cat} using fixed bed system [30].

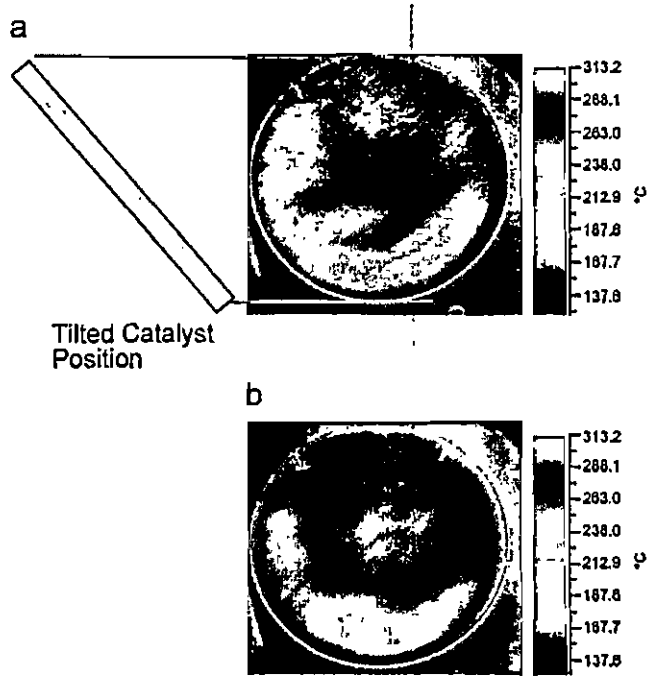

Fig. 3. Thermal profile of the catalyst surface under (a) wet and (b) dry conditions.

5. Reaction conditions for effective dehydrogenation

Due to the endothermic nature of the dehydrogenation of cyclic hydrocarbons chemical equilibrium is favored at higher temperature; the reactions are performed at relatively high temperature under steady-state operations in gas phase. Hodoshima et al. proposed a liquid-film state condition and conducted dehydrogenation of decalin over carbon supported Pt-based catalysts [25,26,28]. Kameyama and coworkers have used a non-steady spray-pulse mode for dehydrogenation of 2-propanol on Pt/α-Al_2O_3 [31]. Ichikawa and coworkers have reported high hydrogen production rates using wet–dry multiphase conditions in batch mode [27,32] and using spray-pulse reactor during dehydrogenation of cyclohexane and decalin over carbon supported Pt. In another publication same group has reported highly efficient production of hydrogen without CO_2 emission in the dehydrogenation of cyclic hydrocarbons under a non-steady spray-pulse operation over supported Pt and Pt–M (M = Re, Rh, Pd) catalysts. Cyclohexane, methylcyclohexane, tetralin and decalin were dehydrogenated by the Pt-containing catalysts supported on thin active carbon cloth sheets and alumite (anodized aluminum) plates. Production rate of hydrogen under the spray-pulse mode is reported to be higher than the conventional batch-type liquid phase reaction and the steady state gas phase reaction in the flow system. Production rate of hydrogen was dependent on the rate of reactant feed, the reaction temperature and the support. Retardation by products adsorbed on the catalysts was negligible under the spray-pulse operation.

Hodoshima et al. [28] reported efficient hydrogen supply from tetralin with superheated liquid-film-type catalysis and using catalysts namely Ni/C, Ru/C and Ni–Ru for operating fuel cells.

The heat transfer to the catalyst and providing required endothermic energy is a key issue for higher catalytic activity in terms of higher hydrogen evolution rates. Biniwale et al. has studied thermal profile of catalysts surface under spray-pulsed injection of cyclohexane over Pt catalysts supported on activated carbon and alumite. Spray-pulsed injection of reactant resulted in higher temperatures periodically on the catalysts surface as revealed from the temperature profiles shown in Fig. 3 This helped in maintaining higher catalytic activity.

6. Patents available

Several patents have appeared claiming use of chemical hydrides including various solid hydrides, liquid hydrides and particularly LOH. Solid hydrides such as $NaBH_4$, $LiBH_4$, KBH_4, $RbBH_4$ are reported for storage of hydrogen effectively [33]. The chemical hydride hydrogen generation system here uses the solute, which is selected from the group consisting of $NaBH_4$, $LiBH_4$, KBH_4, $RbBH_4$. A similar method of generating and storing hydrogen has been disclosed in world patent WO 01/51410 using a chemical hydride solution, such as $NaBH_4$ [34]. As described in this patent, chemical hydride reacts with water in the presence of a catalyst to generate hydrogen. The drawback of these methods is relatively low hydrogen content as compared to possible storage in cycloalkanes and irreversible dehydrogenation leading to no-recycling of the hydrides.

Another class of chemical hydrides reported in various prior arts is liquid organic hydride. Hydrogen evolution during dehydrogenation of methylcyclohexane, decalin, dicyclohexyl and cyclohexane to toluene, naphthalene, biphenyl and benzene,

respectively, in the presence of iridium-based molecular complex catalyst is disclosed [35].

The storage and release of hydrogen by means of a substantially reversible catalytic hydrogenation of extended pi-conjugated substrates is described in US Patent 20050002857 [36]. The pi-conjugated substrates include large polycyclic aromatic hydrocarbons, polycyclic aromatic hydrocarbons with nitrogen heteroatoms, polycyclic aromatic hydrocarbons with oxygen heteroatoms, polycyclic aromatic hydrocarbons with alkyl, alkoxy, nitrile, ketone, ether or polyether substituents, pi-conjugated molecules comprising five membered rings, pi-conjugated molecules comprising six and five membered rings with nitrogen or oxygen heteroatoms, and extended pi-conjugated organic polymers. The hydrogen storage capacity obtained was in the range of 1–4.7% by weight which is relatively low for economical use of these chemicals.

Use of benzene, toluene, xylene, mesitylene, naphthalene, anthracene, biphenyl, phenanthrene and their alkyl derivatives as possible aromatic substrates for producing hydrogen for fuel cells has been reported in Japanese patents [37,38]. Whereas, in another Japanese patent [39] hydrogen storage and supply system is described with catalyst containing at least one metal selected from Ni, Pd, Pt, Rh, Ir, Ru, Mo, Re, W, V, Os, Cr, Co and Fe having good activity for both hydrogenation of hydrogen storage body comprising an aromatic compound and dehydrogenation of a hydrogen supply body comprising the hydrogenated derivative of aromatic compound. A Japanese patent JP2002134141 describes the equipment used for dehydrogenation of LOH with arrangement for intermittent supply of prescribed amount of liquid organic hydride and a product separator for separating hydrogen from other products.

It is apparent, from increasing patent applications in the field of chemical hydrides for storage of hydrogen, that the method has potential for practical applications.

7. Challenges in development of chemical hydrides

Chemical hydrides are definitely potential candidate as hydrogen storage and supply material. However, development of catalyst for selective and efficient dehydrogenation, particularly in case of cycloalkanes, needs to be pursued. Catalyst development also required to target catalytic-reactor configuration to overcome heat transfer limitations for this strongly endothermic reaction. Recycling of chemical hydrides as in case of aromatic–cycloalkanes pairs would be advantageous for reuse of materials; however, the economics has to be worked out for transportation cost in both ways and the weight penalty. Alternatively at the place of delivery of hydrogen, aromatics can be supplied to local chemical industries as solvents.

8. Conclusions

LOH, aromatics–cycloalkanes pairs are potential candidate for high capacity hydrogen storage. Since these can be transported at near ambient conditions may be most useful for long-distance transportation of hydrogen. The endothermic reaction of dehydrogenation can be carried out effectively with advanced reactor systems such as spray-pulsed injection for creating alternate wet and dry conditions over catalyst surface. Development of efficient dehydrogenation catalyst is important particularly considering the cost of Pt-based catalysts. At present the efforts are apparent from recent publications for using minimum amount of Pt for dehydrogenation of cycloalkanes. As LOH can be recycled or alternatively aromatics can be supplied as solvent to chemical industries, this method of hydrogen storage and supply would be economically feasible.

References

[1] Ananthachar V, Duffy JJ. Efficiencies of hydrogen storage systems onboard fuel cell vehicles. Solar Energy 2005;78:687.
[2] David E. An overview of advanced materials for hydrogen storage. J Mater Process Technol 2005;162–3:169.
[3] Singh BK, Singh AK, Srivastava ON. Improved hydrogen sorption characteristics in $FeTi_{1+x}$Mm material. Int J Hydrogen Energy 1996; 21(2):111.
[4] Latroche M. Structural and thermodynamic properties of metallic hydrides used for energy storage. J Phys Chem Solids 2004;65:517.
[5] Ikeda K, Kogure Y, Nakamori Y, Orimo S. Reversible hydriding and dehydriding reactions of perovskite-type hydride $NaMgH_3$. Ser Materialia 2005;53(3):319.
[6] Muthukumar P, Prakash Maiya M, Srinivasa Murthy S. Experiments on a metal hydride-based hydrogen storage device. Int J Hydrogen Energy 2005; 30 (15): 1569.
[7] Singh AK, Singh AK, Srivastava ON. On the synthesis of the Mg_2Ni alloy by mechanical alloying. J Alloys Compd 1995;227:63.
[8] Vijay R, Sunderesan R, Maiya MP, Srinivasa Murthy S. Comparative evaluation of Mg–Ni hydrogen absorbing materials prepared by mechanical alloying. Int J Hydrogen Energy 2005;30:501.
[9] Sandrock G. A panoramic overview of hydrogen storage alloys from a gas reaction point of view. J Alloys Compd 1999; 293–5:877.
[10] Simonyan VV, Johnson JK. Hydrogen storage in carbon nanotubes and graphitic nanofibres. J Alloys Compd 2002; 330–2:659.
[11] Hirscher M, Becher M, Hauska M, Quintel A, Skakalova V, Choi YM et al. Hydrogen storage in carbon nanostructures. J Alloys Compd 2002; 330–2:654.
[12] Darkrim FL, Malbrunot P, Tartaglia GP. Review of hydrogen storage by adsorption in carbon nanotubes. Int J Hydrogen Energy 2002;27:193.
[13] Sankaran M, Kalaiselvan A, Ganesan R, Venuvanalingam P, Viswanathan B. Heteroatom substituted carbon nanotubes: Can they be the activating centers for hydrogen adsorption. Bull Cat Soc India 2002;1:167.
[14] Viswanathan B, Sankaran M, Scibioh MA. Carbon nanomaterials—are they appropriate candidates for hydrogen storage? Bull Cat Soc India 2003;2:12.
[15] Becher M, Hauska M, Hirscher M, Quintel A, Skakalova V, Weglikowska UD et al. Hydrogen storage in carbon nanotubes. C R Phys 2003;4:1055.
[16] Fujii H, Shin O. Hydrogen storage properties in nano-structured magnesium- and carbon-related materials. Physica B:Condensed Matter 2003;328:77.
[17] Fakioglu E, Yurum Y, Veziroglu TN. A review of hydrogen storage systems based on boron and its compounds. Int J Hydrogen Energy 2004;29:1371.
[18] Kojima Y, Kawai Y, Nakanishi H, Matsumoto S. Compressed hydrogen generation using chemical hydride. J Power Sources 2004;135(1–2):36.
[19] Jouthimurugesan K, Bhatia S, Srivastava RD. Kinetics of dehydrogenation of methylcyclohexane over a platinum–rhenium–alumina catalyst in the presence of added hydrogen. Ind Eng Chem Fundam 1985;24(4):433.
[20] Coughlin RW, Kawakami K, Hasan A. Activity, yield patterns, and coking behavior of Pt and PtRe catalysts during dehydrogenation of methylcyclohexane: I. In the absence of sulfur. J Catal 1984;88:150.
[21] Ali JK, Newson EJ, Rippin DWT. Exceeding equilibrium conversion with a catalytic membrane reactor for the dehydrogenation of methylcyclohexane. Chem Eng Sci 1994;49(13):2129.

[22] Taube P, Taube MA. Liquid organic carrier of H_2 as a fuel for automobiles. Adv Hydrogen Energy 1981;2:1077.
[23] Klvana D, Chaouki J, Kusohorsky D, Chavarie C. Catalytic storage of hydrogen: Hydrogenation of toluene over a Nickel/Silica aerogel catalyst in integral flow conditions. Appl Catal 1988;42:121.
[24] Grünenfelder NF, Schucan TH. Seasonal storage of hydrogen in liquid organic hydrides: description of the second prototype vehicle. Int J Hydrogen Energy 1989;14:579.
[25] Hodoshima S, Hiroshi A, Yasukazu S. Liquid-film-type catalytic decalin dehydrogeno-aromatization for long-term storage and long-distance transportation of hydrogen. Int J Hydrogen Energy 2003;28:197.
[26] Hodoshima S, Hiroshi A, Shigeki T, Yasukazu S. Catalytic decalin dehydrogenation/naphthalene hydrogenation pair as a hydrogen source for fuel-cell vehicle. Int J Hydrogen Energy 2003;28:1255.
[27] Kariya N, Fukuoka A, Ichikawa M. Efficient evolution of hydrogen from liquid cycloalkanes over Pt-containing catalysts supported on active carbons under "wet-dry multiphase conditions". Appl Catal A Gen 2002;233:91.
[28] Hodoshima S, Hiroaki N, Yasukazu S. Efficient hydrogen supply from tetralin with superheated liquid-film-type catalysis for operating fuel cells. Appl Catal A Gen 2005;292:90.
[29] Biniwale RB, Nobuko K, Masaru I. Dehydrogenation of cyclohexane over Ni based catalysts supported on activated carbon using spray pulsed reactor and enhancement in activity by addition of a small amount of Pt. Catal Lett 2005;105(1–2):83.
[30] Yoshimi O, Eiji S, Watanabe E, Hyodo S, Nishijima S. Development of dehydrogenation catalyst for hydrogen generation in organic chemical hydride method. Int J Hydrogen Energy 2006;31:1348.
[31] Kobayashi I, Yamamoto K, Kameyama H. A proposal of a spray pulse operation for liquid film dehydrogenation. Chem Eng Sci 1999;54:1319.
[32] Kariya N, Fukuoka A, Utagawa T, Sakuramoto M, Goto Y, Ichikawa M. Efficient hydrogen production using cyclohexane and decalin by pulse-spray mode reactor with Pt catalysts. Appl Catal A Gen 2003;247:247.
[33] United States Patent Application 20030014917.
[34] World patent WO 01/51410.
[35] United States Patent No. 6,074,447.
[36] United States Patent No. 20050002857.
[37] Japanese Patent No. JP20001110437.
[38] Japanese Patent No. JP2002134141.
[39] Japanese Patent No. JP2001198469.

Available online at www.sciencedirect.com
SCIENCE DIRECT®
ELSEVIER
Sensors and Actuators B 94 (2003) 36–45
SENSORS AND ACTUATORS B CHEMICAL
www.elsevier.com/locate/snb

附件二

Investigation of the relationship between surface thermodynamics of the chemically synthesized polypyrrole films and their gas-sensing responses to BTEX compounds

C.W. Lin*, Y.L. Liu, R. Thangamuthu

Department of Chemical Engineering, National Yunlin University of Science and Technology, Yunlin, Taiwan, ROC

Received 28 October 2002; accepted 18 February 2003

Abstract

Cl^--doped polypyrrole (*PPyCl*) films as sensing materials were prepared chemically using $FeCl_3$ as an oxidant and were used to detect benzene, toluene, ethylbenzene, and xylene (BTEX) compounds in their vapor phases, which were found to be able to enhance the doping level of *PPyCl* and hence increased the conductivity of *PPyCl* upon exposure to them. Three isomers of xylene, i.e. ortho (*o*), meta (*m*), and para (*p*), were also investigated for comparison. The sensitivities of *PPyCl* sensor exposed to BTEX compounds with various concentrations were measured and found to lie in the range of 0.08 mΩ/ppm (benzene)–0.8 mΩ/ppm (*o*-xylene). An adsorption model based on the Langmuir isotherm correlated well with the experimental results and was used to interpret the sensing behavior of *PPyCl* sensor towards BTEX vapors. The adsorption equilibrium constants, K_m, were therefore able to be determine according to this model. A further study of affinity between the interested BTEX compound and the *PPyCl* surface was carried out by a method of inverse gas chromatography (IGC) with *PPyCl*-coated glass beads packed in a column as the stationary phase and the interested BTEX compound as the mobile phase. The retention volumes for these compounds were measured to be in the following order: *o*-xylene > *m*-xylene > *p*-xylene ≅ ethylbenzene > toluene. This magnitude sequence was correlated well with that of the equilibrium constants K_m. The free energy of adsorption ΔG_a, consisting of dispersive term ΔG_a^d and the term of acid–base interaction ΔG_a^s, was also determined according to the results obtained from IGC and was used to interpret the sensing response. The interaction forces were analyzed in details by a method of linear solvation energy relationships (LSERs), by which the surface of the *PPyCl* was found to exhibit a basic nature.

Keywords: Polypyrrole; Gas sensor; BTEX; Inverse gas chromatography; Free energy of adsorption; Linear solvation energy relationships

1. Introduction

It is well known that electron-conducting polymers can be used as chemical sensors by measuring the conductivity changes as a function of secondary doping or undoping of detected species [1–6]. Polypyrrole (*PPy*) was initially used to measure the response to ammonia vapor by Nylander et al. [1] in 1983. Later, the similar device was used to measure the responses to other gases [2–6] under suitable conditions; presumably these gases reacted with *PPy* by oxidizing and reducing the *PPy*, respectively. In order to improve the characteristics of *PPy* film, several *PPy*-based composites as gas sensors had been studied [7–12]. Hwang et al. [13] have proposed a microscopic gas-sensing model indicating that the sensitivity of the sensor depends on the site number of a monolayer, the thickness of the sensing film, the adsorption equilibrium constant as well as the change of site resistance. We utilized this microscopic adsorption model to explain the sensing behaviors of the conducting polymer sensors and also endeavored to make correlation between sensing parameters and the experimental results to give an interpretation for the different responses.

Recently, the attention of various air pollution control agencies has been increasingly focused on the control of volatile organic compounds (VOCs). Considerable quantities of VOCs are produced from industrial sources such as printing and coating facilities, foundries, electronics, and paint manufacturing units. A group of VOCs, including aromatic hydrocarbons such as benzene, toluene, ethylbenzene, and xylene (BTEX), are widely used in industry and poses serious adverse effects on the quality of air. The utilization of conducting polymers as gas sensors for detecting these highly health-threatening VOCs may be a promising approach. We have previously presented the results of sensing

* Corresponding author. Tel.: +886-5-534-2601x4613; fax: +886-5-531-2071.
E-mail address: lincw@pine.yuntech.edu.tw (C.W. Lin).

0925-4005/03/$ – see front matter © 2003 Elsevier Science B.V. All rights reserved.
doi:10.1016/S0925-4005(03)00323-X

responses of electrochemically prepared $PPyClO_4$ sensors exposed to BTEX compounds [14]. The effect of adsorption affinity and the undoping efficiency could be distinguished and calculated in terms of adsorption equilibrium constant. We obtained a good correlation between the adsorption equilibrium constant and the measured sensitivity and concluded that the affinity of the interested compound to the sensing layer dominated the sensing response in our work.

Although the development of gas sensors based on the organic conducting polymers is plausible, the exact nature of the interactions between the analyte molecules and the conducting polymer surface remain largely unknown. Identification of the interactions undergone at the sensor–gas interface is crucial for the design and selection of future sensor materials. In the past, various techniques [15–22] have been used to investigate surfaces of conducting materials. Amongst these techniques, inverse gas chromatography (IGC) appears to be particularly useful for determining the sorption properties of molecules on surface. Chehimi et al. [21,22] investigated surfaces of conducting materials using IGC with packed column and reported that the surface to be amphoteric, i.e. polar molecules (Lewis acids and bases) adsorbed to a greater degree of the surface than to non-polar molecules, and the preparation condition of the polymer played a vital role in the surface thermodynamics of the polymer.

The present work is a continuation of our earlier studies on the development of gas sensors based on organic conducting polymer films, and is devoted to investigate the gas-sensing behaviors of chemically prepared Cl^--doped polypyrrole (*PPyCl*) sensor exposed to BTEX compounds. Beside this, we also intend to present some preliminary results obtained using IGC technique subjected to the relationship of the surface interaction force and the sensing response.

2. Experimental

2.1. Preparation of PPy sensing layer

An interdigitated gold electrode screen-printed onto the surface of an alumina substrate was used. Its structure and dimensions were the same as in the earlier reports [11,12]. Chemiresistors were fabricated by deposition of these electrodes with *PPy* thin film. Polymerization of pyrrole was carried out by a chemical oxidation using $FeCl_3$ as an oxidant. The alumina substrate with interdigitated Au electrode was immersed into the $FeCl_3$ solution for 1.0 h and then immersed in pyrrole solution for polymerization for 30 min.

2.2. Measurement of resistance change of PPyCl

The resistance change of *PPyCl* film due to the exposure of BTEX compounds (with N_2 mixture with purity level 99.99%) were measured using a device mainly consisting of the current–voltage (*I–V*) meter and an automatic data acquisition system. Resistance measurements were taken when the response was maximum and constant. All BTEX samples were obtained from Aldrich (HPLC grade) and used without any further purification.

2.3. Inverse gas chromatography

2.3.1. Preparation of stationary phase of IGC

Glass beads (60 meshes) weighted totally about 0.5 g were ultrasonic cleaned in a water bath containing non-ionic surfactant. This weight was suitable for packing a 2 m long column with 1/8 in. in diameter. The pre-cleaned glass beads were then immersed in 14 mM $FeCl_3$ oxidant solution and were slightly stirred for about 1 h to make $FeCl_3$ be adsorbed homogencously on the glass beads. The pre-treated glass beads were then transferred into a beaker containing pre-distilled pyrrole monomer kept at a constant temperature of 6 °C and were gently stirred for 12 h for chemical oxidation in solution. The *PPy*-coated glass beads were then washed with methanol to remove excess oxidant and vacuum-dried at 45 °C for 24 h.

2.3.2. Measurements of IGC data

Measurements were carried out with a China Chromatography 8900 gas chromatograph fitted with a flame ionization detector. High purity grade nitrogen was used as the carrier gas. The flow rate was 62 ml min^{-1} as measured by a soap-bubble flow meter. Oven temperature was varied from 423 to 443 K. The carrier gas flow rate was adjusted at each temperature to maintain a constant flow rate over the temperature range studied. The column inlet pressure (P_i) was 1.60 bar and the outlet pressure (P_o) was atmosphere. The injector and detector zones were kept at 463 K to minimize temperature gradients in these areas. The stationary phase was conditioned for 8 h prior to chromatographic measurements. Probes were injected manually at least in triplicate by a gas-tight Hamilton syringe. To achieve extreme dilution of the probes, the syringe was purged as many times as necessary. The signals were recorded with a digital recorder and the retention times were calculated graphically [23] and corrected the dead time t_0 for the column using air as an non-interacting marker.

Non-polar samples for a dispersion interaction reference state included C_6–C_9 *n*-alkanes were obtained from Aldrich (HPLC grade) and used without any further purification. All other BTEX samples are same as those used in the sensitivity measurements.

2.3.3. Data analysis

In IGC, measurements were carried out at infinite probe dilution, i.e. approximately zero sorbent surface coverage, ensure that the results obtained from the experiments apply exclusively to adsorbate–adsorbent interactions. The retention time of the probe, t_r, the time it takes the probe to travel through the column, can be converted to the net retention

volume V_N, by [24]

$$V_N = JF(t_r - t_0) = JFt_n \quad (1)$$

where F is the carrier gas flow rate, t_n the net retention time, and J the correction factor of pressure gradient for mobile phase

$$J = \frac{3(P_i/P_o)^2 - 1}{2(P_i/P_o)^3 - 1} \quad (2)$$

The value of J was calculated to be 0.7625 in the present study. The net retention volume, V_N is related to the free energy of adsorption, ΔG_a ($J\,mol^{-1}$) by [25]

$$\Delta G_a = -RT\ln(V_N) + C \quad (3)$$

where R is the gas constant, T the column temperature, and C, a constant which takes into account the weight and specific surface area of the packing material and the standard states of the probes in the mobile and the adsorbed states [26]. Manipulation of ΔG_a (or $RT\ln(V_N)$) data for the various probes leads to the evaluation of γ_s^d, the dispersive contribution to the surface energy of the materials.

2.3.4. Dispersive contribution to the surface energy

A standard method to evaluate γ_s^d, the dispersive component of the surface energy, relies on the retention data of the n-alkane series [27]. Practically for these probes, ΔG_a or simply $RT\ln(V_N)$ values are plotted against n_C, the number of carbon atoms in the n-alkane molecules, and the slope of the linear correlation refers to ΔG^{CH_2}, the free energy of adsorption of a methylene group.

$$\gamma_s^d = \frac{1}{4}\gamma^{CH_2}\left(\frac{\Delta G^{CH_2}}{Na_{CH_2}}\right) \quad (4)$$

where N is the Avogadro number, a_{CH_2} is the cross-sectional area of an adsorbed CH_2 group (6 Å^2), and γ^{CH_2} is the surface energy of the solid containing only methylene groups such as polyethylene ($\gamma^{CH_2} = 36.8 - 0.058T$ (°C)) [27].

2.3.5. Specific interactions

If both dispersive and specific interactions are operative at the gas/solid interface, it is assumed that they contribute to the total ΔG_a in a additive manner:

$$\Delta G_a = \Delta G_a^d + \Delta G_a^s \quad (5)$$

where 'd' and 's' are referred to dispersive and specific interactions, respectively. Several approaches were proposed to distinguish between ΔG_a^d and ΔG_a^s [28]. In the present investigation, we use the traditional approach of Brookman and Sawyer [29] in which ΔG_a or $RT\ln(V_N)$ values are related to the boiling point of the injected probes. The n-alkanes series lead to a reference linear correlation, and for polar probes interacting specifically with stationary phase, or $RT\ln(V_N)$ values deviate from the linear correlation defined by the n-alkanes. For a given polar probe, the vertical distance from the reference line yields:

$$-\Delta G_a^s = RT\ln(V_N/V_{N,ref}) \quad (6)$$

where $V_{N,ref}$ is the net retention volume of a hypothetical n-alkane that boils at the same temperature as the rest polar probe.

2.3.6. Application of solvation equations to IGC data

From earlier research, solvation equations using sample, or solute parameters as descriptors can be applied to the correlation and prediction of adsorption phenomena. The phenomena may include specific retention volume, $\log(V_g)$ [30,31], or gas–liquid partition coefficients [32–34] on various adsorbents. The general linear solvation energy relationship (LSER) equation can be described as follows:

$$\log(SP) = c + rR_2 + s\pi_2^H + a\alpha_2^H + b\beta_2^H + l\log(L^{16}) \quad (7)$$

where SP is the experimental data, R_2 the solute excess molar refraction that reflects the ability of solute to interact with sorbent through π- and n-electron pairs; π_2^H is the solute dipolarity–polarisability, a measure of the dipole–dipole or dipole-induced dipole interactions; α_2^H and β_2^H the effective hydrogen-bond acidity and basicity of the solute and L^{16} the solute gas–liquid partition coefficient of hexadecane at 298 K, a measure of dispersion interactions. All the parameters, except R_2, are derived from thermodynamical data of partitioning and/or complexation equilibria. The constants c, r, s, a, b, and l are found by multiple linear regression analysis. Eq. (7) allows the surface to be described in terms of specific chemical properties. Consequently, straightforward interpretation of the IGC data can be applied in terms of the surface chemistry of *PPyCl*. The statistical analysis and the LSER descriptors calculations were carried out with minitab software.

3. Results and discussion

3.1. Interaction mechanisms of electron-donating gases with PPyCl

PPy is a n-type semiconductor when doped with Cl^-. Therefore, the exposure of electron-donating gases such as ammonia and alcohol, to *PPyCl* causes an increase in conductance, i.e. a decrease in resistance. The recovery of the conducting polymer to its initial oxidized state is ascribed to desorption, by flushing with N_2, of the nucleophiles. The interaction between *PPyCl* and electron-donating compound is generally considered to be a doping effect. Thus, p-type dopants can increase the doping level of the polymer chain by enhancing the effect of the original dopant.

3.2. Responses of PPyCl sensor to BTEX compounds

o-Xylene is an electron-donating compound, when exposed which causes an increase in the conductivity of the chemically prepared *PPyCl* sensor film. As a gas-sensing test, we used on–off cycles at 67 ppm concentration of *o*-xylene to study the gas-sensing behavior of *PPyCl* film.

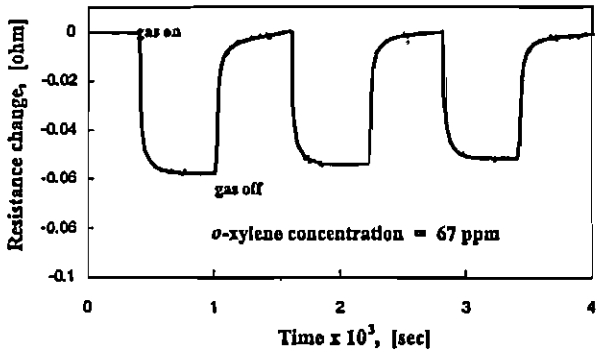

Fig. 1. Several on–off cycles to study the reproducibility of the sensing behavior of *PPyCl* film to *o*-xylene vapor at 67 ppm.

As can be seen in Fig. 1, a reasonable reproducibility was obtained. However, a minor drift of baseline was observed. As shown in Fig. 2, the resistance change (ΔR) becomes greater as the *o*-xylene concentration increased in steps from 20 to 60 ppm in N_2. Also at *o*-xylene concentration of 60 ppm, the sensor responded as quickly as in about 60 s. The response times were about 200 to 400 s for concentrations lower than 60 ppm. In contrast, vapors of higher concentration (60 ppm) took longer time (585 s) to recover from the oxidized state. A plot of resistance changes of *PPyCl* sensor vs. *o*-xylene concentration was given in Fig. 3. It is clear from the plot that the resistance change is linearly proportional to the *o*-xylene concentration. The slope of the linear plot represents the sensitivity of the sensor characterized as the resistance change per unit *o*-xylene concentration. The sensitivity of the *PPyCl* sensor to *o*-xylene vapor was 0.8 mΩ/ppm.

Ethylbenzene is another electron-donating compound which also causes an increase in the conductivity of the *PPyCl* sensor. As a gas-sensing test, we used on–off cycles at 90 ppm concentration of ethylbenzene to study the gas-sensing behavior of *PPyCl* film. As can be seen in Fig. 4, a reasonable reproducibility can be noticed. However, a small drift of baseline was observed. As shown in Fig. 5, the signal of resistance change becomes greater as the ethylbenzene concentration increased in steps from 20 to 90 ppm. The response times for ethylbenzene were ranged from 180 to 460 s. Compared to *o*-xylene (Fig. 2), the response speed of ethylbenzene (Fig. 5) was very slow. At the same time, compared to recovery speeds of ethylbenzene, desorption of *o*-xylene from *PPyCl* film was much slower manifesting the interaction between the *o*-xylene was stronger than that with ethylbenzene. This observation may imply that *o*-xylene had a better affinity towards *PPyCl* film. The resistance changes of *PPyCl* sensor plotted against ethylbenzene concentration are shown in Fig. 6. It can be seen that resistance change varies linearly with ethylbenzene concentration. A sensitivity of 0.4 mΩ/ppm was obtained from the slope of the linear plot.

With *PPyCl* sensor, a similar procedure was followed for the detection of vapors of other two xylene isomers namely *m*-xylene and *p*-xylene. As shown in Fig. 7, the resistance changes are linearly proportional to concentrations of these two isomers. The sensitivities obtained from the linear plots were 0.6 mΩ/ppm for both *m*-xylene and *p*-xylene. Similarly, the sensitivity obtained from linear plot of ΔR vs. concentration for benzene vapor (not shown in Fig. 7) in the concentration range of 200–500 ppm was 0.08 mΩ/ppm. The sensitivities obtained with *PPyCl* sensor for BTEX compounds

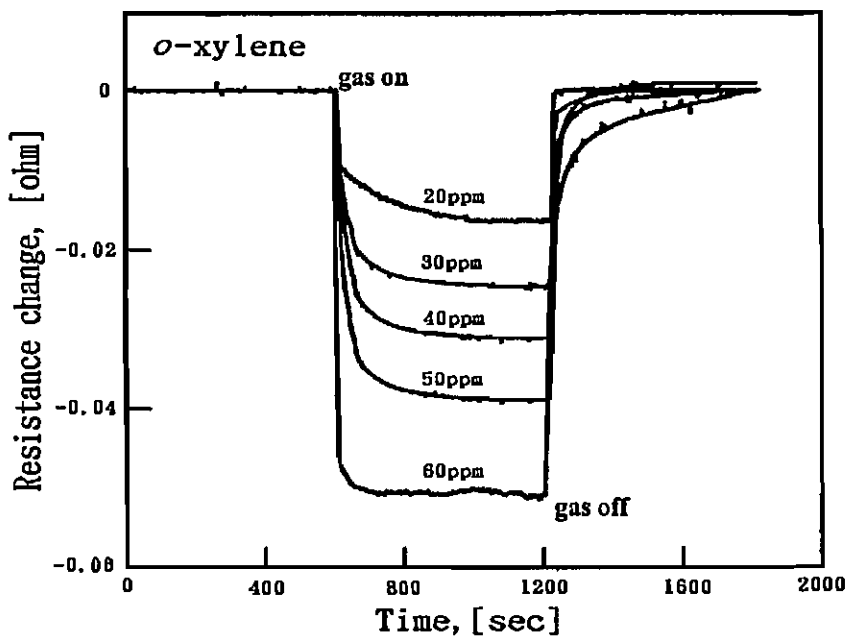

Fig. 2. Change in resistance, ΔR caused by increasing *o*-xylene concentration in steps from 20 to 60 ppm in N_2.

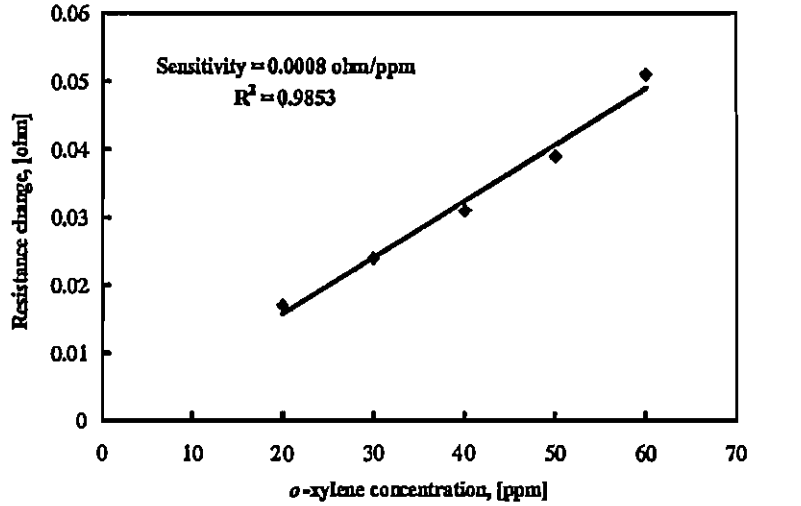

Fig. 3. Change in resistance, ΔR of the *PPyCl* sensor plotted against *o*-xylene concentration.

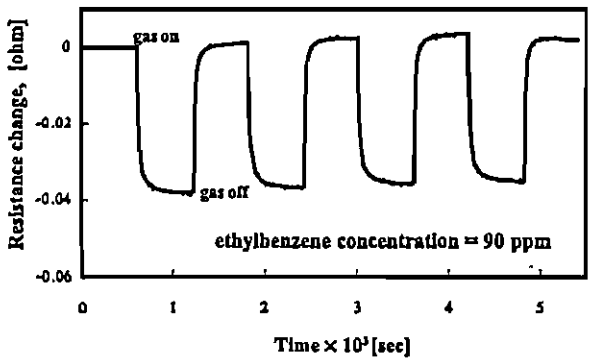

Fig. 4. Several on–off cycles to study the reproducibility of the sensing behavior of *PPyCl* film to ethylbenzene vapor at 90 ppm.

are in the following order:

o-xylene > *m*-xylene
≅ *p*-xylene > ethylbenzene > toluene > benzene

3.3. Calculations of the parameters for the gas-sensing model

Hwang et al. [13] have previously proposed a microscopic gas-sensing model to explain the behaviors of *PPy*-based sensors to electron-donating compounds. The overall resistance of the composite film can be regarded as the paralleling of several pseudo-monolayers and each layer is composed of several resistors in series. In this model, R, r, n, and m

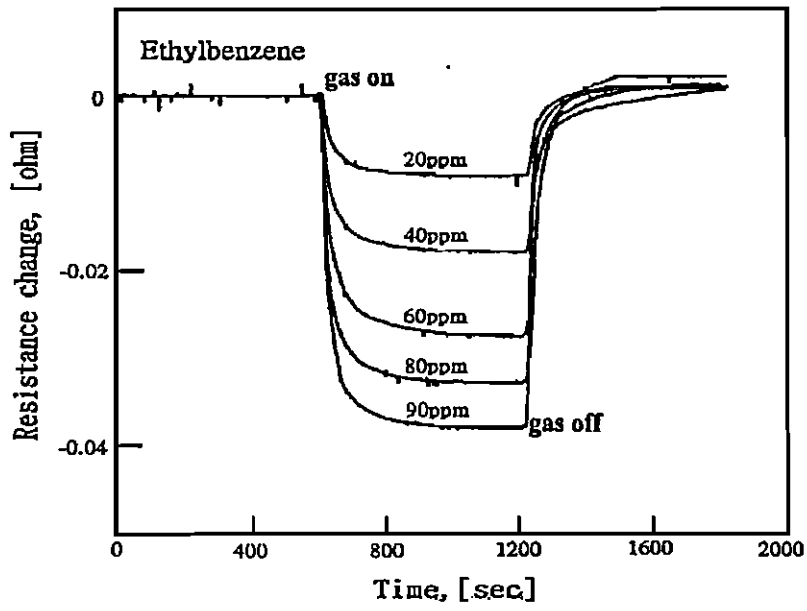

Fig. 5. Change in resistance, ΔR caused by increasing ethylbenzene concentration in steps from 20 to 90 ppm in N_2.

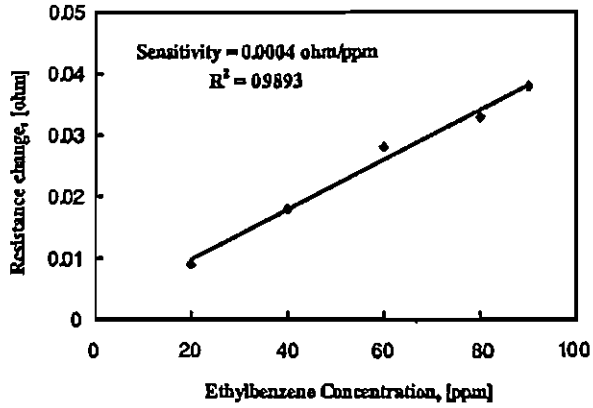

Fig. 6. Change in resistance, ΔR of the *PPyCl* sensor plotted against ethylbenzene concentration.

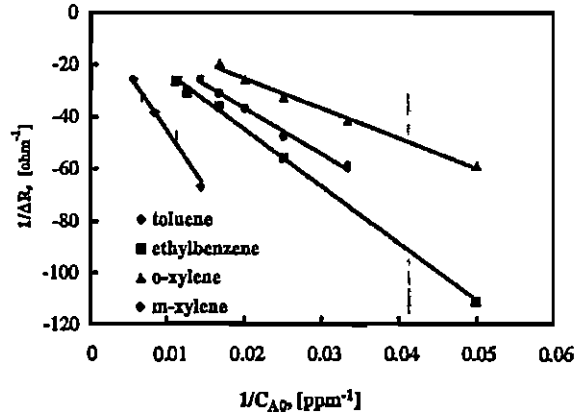

Fig. 8. $1/\Delta R$ vs. $1/C_{A0}$ for *PPyCl* thin film exposed to toluene, ethylbenzene, *o*-xylene, and *m*-xylene vapors.

represents resistance of a monolayer, resistance of an active site, thickness of the thin film, and the number of active sites on a pseudo-monolayer, respectively. It manifests that the plot of reciprocal of the resistance change against the reciprocal of gas concentration is a linear relationship according to the following equation based on the proposed model:

$$\frac{1}{\Delta R} = \frac{n}{m(r_1 - r_0)} + \frac{n}{m(r_1 - r_0)K_m}\frac{1}{C_{A0}} \quad (8)$$

where ΔR is the resistance difference after and before gas sorption, K_m the adsorption equilibrium constant, C_{A0} the concentration of the detected gas, r_1 and r_0 are the site resistance as the site is vacant and occupied, respectively. The value of $[m(r_1-r_0)]/n$ can be determined from the reciprocal of the intercept and K_m can be obtained by dividing the intercept by the slope. It had been previously reported that this model interprets well the bchaviors of *PPy*–PEO [11] and *PPy*–PVA [12] composite sensors exposed to ethanol vapors by comparing the experimental results. An increase in the polymerization charge usually led to a thicker sensing film, i.e. a greater *n*-value, and therefore decreased $[m(r_1-r_0)]/n$ values. However, the thickness (determined by the total electrical charge) was kept constant in this investigation. Fig. 8 shows the plot of $1/\Delta R$ vs. $1/C_{A0}$ for the *PPyCl* thin film exposed to toluene, ethylbenzene, *o*-xylene, and *m*-xylene vapor, respectively. The values of $[m(r_1-r_0)]/n$ and K_m are given in Table 1 for benzene, toluene, ethylbenzene, *o*-xylene, *m*-xylene and *p*-xylene. K_m value was dependent on the affinity of the detected compound to the sensing material (*PPyCl*) and found to follow the order: *o*-xylene (1.97×10^{-3}) > *m*-xylene (1.07×10^{-3}) > *p*-xylene (7.45×10^{-4}) > ethylbenzene (6.50×10^{-4}) > toluene (2.50×10^{-4}) > benzene (1.72×10^{-4}). As the values of *m* (number of active sites on a monolayer) and *n* (number of layers proportional to the thickness of the film) were ideally assumed to be identical (i.e. polymerization conditions and polymerization period), therefore, the affinity of vapor to the conducting material film determine the value of the sorption equilibrium constant K_m. Accordingly, *o*-xylene was the one having the highest affinity to conducting *PPyCl* film among the investigated BTEX compounds. The results of response time and recovery speed also indicate similar phenomena that *o*-xylene vapor had higher affinity. It can also be noticed that there is a correlation between the K_m value and the sensitivity. With increasing K_m value, the sensitivity increases linearly in the lower K_m value region and at higher K_m values, sensitivity increased sharply

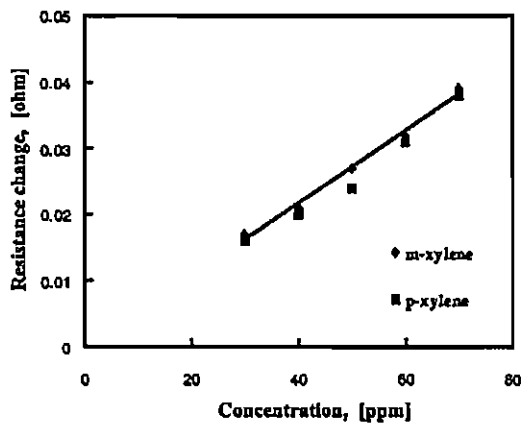

Fig. 7. Change in resistance, ΔR of the *PPyCl* sensor plotted against the concentration of *m*-xylene and *p*-xylene.

Table 1
The values of sensitivity, K_m and $m(r_1 - r_0)/n$ for BTEX vapors detected by *PPyCl* sensor

Vapors	Sensitivity (Ω/ppm)	K_m	$m(r_1 - r_0)/n$ (Ω)
Benzene	8×10^{-5}	1.72×10^{-4}	−0.44
Toluene	2×10^{-4}	2.50×10^{-4}	−0.91
Ethylbenzene	4×10^{-4}	6.50×10^{-4}	−0.70
o-Xylene	8×10^{-4}	1.97×10^{-3}	−0.44
m-Xylene	6×10^{-4}	1.07×10^{-3}	−0.54
p-Xylene	6×10^{-4}	7.45×10^{-4}	−0.71

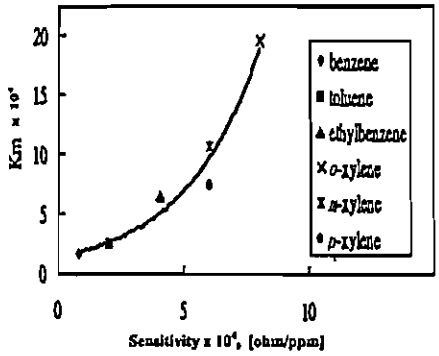

Fig. 9. Plot of K_m ($\times 10^4$) vs. sensitivity ($\times 10^4$) for BTEX vapors detected by *PPyCl* sensor.

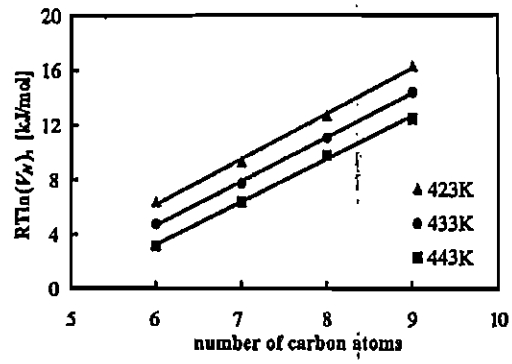

Fig. 10. $RT\ln(V_N)$ vs. number of carbon atoms plot for adsorption of *n*-alkanes on *PPy*.

as shown in Fig. 9. The sensing ability of the conducting polymer film depended on both the secondary doping (or undoping) level by the detected compound and the affinity of the compound to the sensing material. Since there was no regular change in $[m(r_1-r_0)]/n$ values with sensitivity, it can be concluded that in the present case the sensing ability of the conducting *PPyCl* polymer film is dominated by the affinity of the compound to the sensing material rather than the secondary doping (or undoping) level by the detected compound. In order to prove this, the rest of work deals with the study of affinity in terms of the thermodynamic parameters between the chemically prepared *PPyCl* film and BTEX compounds using IGC technique.

3.4. Inverse gas chromatography

$RT\ln(V_N)$ values for *n*-alkane homologous series adsorbed on *PPyCl* at three temperatures are given in Table 2. Fig. 10 shows plots of $RT\ln(V_N)$ vs. n_C, the number of carbon atoms in the alkane molecule at 423, 433, and 443 K. Excellent linear plots are generated showing that the adsorption energy for the *n*-alkanes increases with the number of carbon atoms in the chain. The slope of linear plot is refer to ΔG^{CH_2}, the free energy of adsorption of a methylene group (see Section 2.3.3). It can be seen from the following Eqs. (9)–(11) that in the present study the ΔG^{CH_2} obtained at three temperatures are varied from 3.14 to 3.31 mJ m^{-2} which closely agree with the reported values of 2.6–5.0 mJ m^{-2} [35].

$$443\,\text{K}: \quad RT\ln(V_N) = 3.1361 n_C - 15.555 \tag{9}$$

$$433\,\text{K}: \quad RT\ln(V_N) = 3.21791 n_C - 14.631 \tag{10}$$

$$423\,\text{K}: \quad RT\ln(V_N) = 3.3103 n_C - 13.653 \tag{11}$$

The ΔG^{CH_2} values can be used to calculate γ_s^d values. The results of this calculation are given in Table 3. γ_s^d values are decreased with increase in temperature. This is due to increase in the kinetic energy of the adsorbed molecules on the surface which cause decrease in the surface energy. γ_s^d value of 74.73 mJ m^{-2} for *PPyCl* at 423 K shows that the *PPyCl* is a high surface-energy material compared to conventional polymers [35]. Thus, *PPyCl* have dispersive properties which lie between those for conventional polymers and high surface-energy materials such as metals and graphite. It can obviously be expected a strong interactions between the high surface-energy *PPyCl* adsorbent and polar adsorbate. Therefore such high surface-energy conducting polymer coatings can advantageously be used to fabricate sensors with better sensitivity.

Using the following thermodynamic relation, from the slope of linear plot between γ_s^d vs. T, the dispersive component of enthalpy change ΔH_a and entropy change ΔS_a can be calculated.

$$\Delta G_a = \Delta H_a - T\Delta S_a \tag{12}$$

Table 2
Measured value of $RT\ln(V_N)$ for *n*-alkanes adsorbed onto *PPyCl* at three temperatures

Temperature (K)	Probes	$RT\ln(V_N)$ (kJ/mol)
443	*n*-Hexane	3.168
	n-Heptane	6.393
	n-Octane	9.821
	n-Nonane	12.479
433	*n*-Hexane	4.789
	n-Heptane	7.740
	n-Octane	11.086
	n-Nonane	14.400
423	*n*-Hexane	6.386
	n-Heptane	9.327
	n-Octane	12.687
	n-Nonane	16.300

Table 3
Dispersion component of surface energy for *PPy* determined at three temperatures

	Temperature (K)		
	443	433	423
γ_s^d (mJ/m^2)	69.96	72.10	74.73

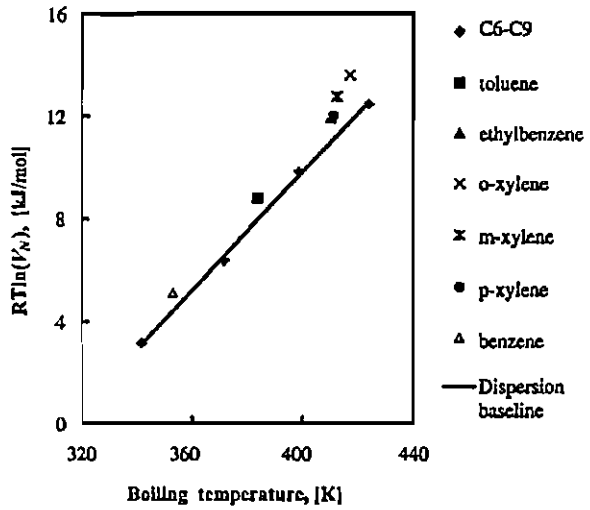

Fig. 11. Plot of $RT\ln(V_N)$ vs. the boiling point for *n*-alkanes and BTEX probes adsorbed onto *PPyCl* at 443 K.

In the present study, the value of enthalpy change, ΔH_a is 175.45 mJ m^{-2} and entropy change, ΔS_a is 0.2383 m^{-2} K^{-1}.

3.5. Adsorption free energies of the probes

Fig. 11 demonstrates $RT\ln(V_N)$ vs. boiling point plot for *PPyCl* at 443 K. The *n*-alkane series lead to a linear plot which constitutes a reference for London dispersive interactions. The marker corresponding to the BTEX compounds are located off the baseline defined by the *n*-alkanes, thus indicating that *PPyCl* behaves amphotically. As mentioned above, the separation of the marker from the baseline was referred to the specific interaction between the interested BTEX compound and the *PPyCl* adsorbent and the distance corresponds to $-\Delta G_a^s$. The adsorption free energies of BTEX compounds are given in Table 4. As can be seen, the negative values of ΔG_a show an order of *o*-xylene > *m*-xylene > *p*-xylene ≅ ethylbenzene > toluene. It can also be noticed that the dispersive component contributed largely to the total free energy of adsorption. On the other hand, the contribution of specific interaction is not significant. However, the specific term also showed a similar order of *o*-xylene > *m*-xylene > ethylbenzene ≅ *p*-xylene > toluene.

Fig. 12 illustrates the variation of adsorption equilibrium constant, K_m with $-\Delta G_a^s$. It can be noticed an excellent linear correlation between K_m and $-\Delta G_a^s$ i.e. specific interaction between the BTEX compounds and *PPyCl* surface. This observation is an experimental proof to our earlier conclusion from the resistance measurements that the affinity (i.e. the coverage) of the detected vapor to the sensing material dominated the sensitivity of the gas sensor in the present study.

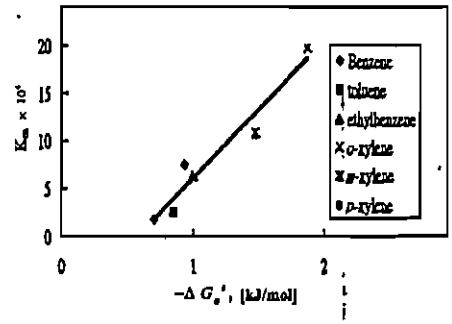

Fig. 12. Plot of K_m ($\times 10^4$) vs. specific adsorption energy for BTEX vapors.

Table 5
Values of various probes parameters [36]

Probes	$\log(V_N)$	R_2	π	$\sum\alpha$	$\sum\beta$	$\log(L^{16})$
Benzene	0.666	0.61	0.52	0	0.14	1.786
Toluene	1.036	0.601	0.52	0	0.14	3.325
Ethylbenzene	1.407	0.613	0.51	0	0.15	3.778
o-Xylene	1.605	0.663	0.56	0	0.16	3.939
m-Xylene	1.495	0.623	0.52	0	0.16	3.839
p-Xylene	1.418	0.613	0.52	0	0.16	3.839
C6	0.374	0	0	0	0	2.668
C7	0.754	0	0	0	0	3.173
C8	1.158	0	0	0	0	3.677
C9	1.472	0	0	0	0	4.182
Methanol	0.293	0.278	0.43	0.43	0.47	0.970
Ethanol	0.615	0.246	0.37	0.37	0.48	1.485
Water	1.401	0	0.82	0.82	0.35	0.260

3.6. Application of solvation equations to IGC data

Retention volumes of 13 probes have been obtained by the IGC method. Using retention volume and LSER parameters of solutes, a multiple linear regression analysis was carried out. The data are given in Table 5, and the LSER equation is given below.

$$\log(V_N) = -1.72 - 2.04R_2 + 3.11\pi + 2.29\sum\alpha - 1.04\sum\beta + 0.775\log(L^{16}),$$
$$n = 12,\ r = 0.992 \qquad (13)$$

Table 4
Values of $-\Delta G_a$, $-\Delta G_a^d$, and $-\Delta G_a^s$ for BTEX probes adsorbed onto *PPyCl*

Free energy of adsorption (kJ/mol)	Benzene	Toluene	Ethylbenzene	*o*-Xylene	*m*-Xylene	*p*-Xylene
$-\Delta G_a$	5.12	8.79	11.93	13.61	12.68	12.02
$-\Delta G_a^d$	4.42	7.94	10.94	11.75	11.21	11.06
$-\Delta G_a^s$	0.70	0.85	0.99	1.86	1.47	0.94

Table 6
$\log(V_N)$ values of benzene obtained from IGC experiment and LSER calculations

	LSER (theoretical)	IGC (experimental)
$\log(V_N)$ (min)	0.666	0.604

Predictions can be made regarding the activity of the *PPyCl* surface by examining the constants in the above equation. The largest coefficient is that for π the dipolarity–polarisability of the solute, a measure of the ability of a molecule to stabilize a neighboring charge or dipole. This observation indicates that the presence of nitrogen and/or chlorine in the polymer may lead to the formation of dipoles within the *PPy* layer, with which solute molecules may interact. Due to this polar nature of *PPyCl* surface, non-polar benzene vapor gives low sensitivity (0.008 mΩ/ppm) compared to high sensitivity (0.08 mΩ/ppm) of polar *o*-xylene vapor.

The constant for α indicates that the *PPyCl* surface exhibits largely basic nature. The negative constant for β reinforces this, denoting that solutes with a hydrogen-bond basic nature would experience repulsive forces. Such basic nature would be expected from the electron-rich structural features of *PPy* due to conjugated backbone of carbon and nitrogen. Again a negative value for coefficient R_2 indicates a repulsive force experienced by the solutes with large *n*- and π-electronic characters.

In order to test the validity of the LSER treatment, the calculated value from this treatment was compared with the experimental value. It can be seen from Table 6 that retention volume of benzene obtained from experiment is 0.604 which is comparable with 0.666 calculated using LSER. There is about 9.4% differences between the two values showing the validity of LSER approach in the present investigation.

4. Conclusions

The sensing responses of the Cl^--doped *PPy* sensors towards BTEX compounds were investigated. It was found that the *PPyCl* thin film deposited on a pair of suitable interdigitated electrodes could be used to detect BTEX vapors reliably by measuring the resistance change of the film. The sensitivity of *PPyCl* sensor for BTEX compounds are found to lie in the range of 0.08 mΩ/ppm (benzene)–0.8 mΩ/ppm (*o*-xylene). A linear relationship of $1/\Delta R$ plotted against $1/C_{A0}$ was obtained from the theoretical considerations and was correlated well with the experimental results. The adsorption equilibrium constants, K_m, calculated according to the adsorption theory, were in a magnitude order of *o*-xylene (1.97×10^{-3}) > *m*-xylene (1.07×10^{-3}) > *p*-xylene (7.45×10^{-4}) > ethylbenzene (6.50×10^{-4}) > toluene (2.50×10^{-4}) > benzene (1.72×10^{-4}). A good correlation between the sensitivity and K_m values was obtained. The interactions between the BTEX compounds and the sensing material were further evaluated using IGC technique. A good correlation between the adsorption equilibrium constants, K_m, and specific component of free energy of adsorption, $-\Delta G_a^s$, substantiate the fact that the affinity (i.e. the coverage) of the detected BTEX vapor to the sensing material dominated the sensitivity of the gas sensor in the present work. From the detailed analysis of the interaction forces by LSERs, it was found that the surface of the *PPyCl* was basic in nature.

Acknowledgements

This work was financially supported by the National Science Council of the Republic of China, Taiwan (Grant NSC-90-2214-E-224-007) and Ministry of Education, Taiwan (Grant EX-91-E-FA 09-5-4).

References

[1] C. Nylander, M. Armgrath, I. Lundstorm, in: Seiyama et al. (Eds.), An Ammonia Detector Based on a Conducting Polymer in Chemical Sensor, Proceedings of the International Meeting on Chemical Sensors, Fukuoka, Japan, Elsevier, Kodansha, 1983, pp. 203–207.
[2] P.N. Bartlett, S.K. Ling-Chung, Sens. Actuators 19 (1989) 141.
[3] P.N. Bartlett, S.K. Ling-Chung, Sens. Actuators 20 (1989) 287.
[4] P.N. Bartlett, P.B.M. Archer, S.K. Ling-Chung, Sens. Actuators 19 (1989) 125.
[5] I. Lahdesmaki, A. Lewenstam, A. Ivaska, Talanta 43 (1996) 125.
[6] N.M. Ratchiffe, Anal. Chim. Acta 239 (1990) 257.
[7] J.P. Blanc, G. Blasquez, L.P. Germain, A. Larbi, C. Maleysson, H. Robert, Sens. Actuators 14 (1988) 143.
[8] M.D. Paoli, R.J. Waltman, A.F. Diaz, J. Bargon, J. Chem. Soc. Chem. Commun. (1984) 1015.
[9] G. Hailin, L. Yucheng, Sens. Actuators B 21 (1994) 57.
[10] P. Bruschi, F. Cacilli, A. Nannini, Sens. Actuators A 32 (1992) 313.
[11] C.W. Lin, C.R. Lee, B.J. Hwang, Mater. Chem. Phys. 55 (1998) 139.
[12] C.W. Lin, B.J. Hwang, C.R. Lee, J. Appl. Polym. Sci. 73 (1999) 2079.
[13] B.J. Hwang, J.Y. Yang, C.W. Lin, J. Electrochem. Soc. 146 (1999) 1231.
[14] C.W. Lin, S.S. Liu, B.J. Hwang, J. Appl. Polym. Sci. 82 (2001) 954.
[15] M.L. Abel, M.M. Chehimi, Synth. Met. 66 (1994) 225.
[16] K.L. Tan, B.T.G. Tan, K. Kang, K.G. Neoh, Y.K. Ong, Phys. Rev. B: Condens. Matter 42 (1990) 7563.
[17] M. Josowicz, J. Janata, K. Ashley, Spons, Anal. Chem. 59 (1987) 253.
[18] J. Li, E. Wang, M. Green, P.E. West, Synth. Met. 74 (1995) 127.
[19] P.R. Teasdale, H. Ge, K. Gilmore, G.G. Wallace, Polym. Int. 29 (1992) 299.
[20] H. Ge, G.G. Wallace, J. Chromat. 588 (1991) 25.
[21] M.M. Chehimi, E. Piogis-Landureau, M. Delamar, J. Chim. Phys. 89 (1992) 1173.
[22] M.M. Chehimi, M.L. Abel, E. Piogis-Landureau, M. Delamar, Synth. Met. 60 (1993) 183.
[23] J.R. Conder, C.L. Young, Physicochemical Measurement by Gas Chromatography, Wiley, Chischester, 1979.
[24] D.R. Lord, T.C. Ward, H.P. Schreiber (Eds.), Inverse Gas Chromatography: Characterization of Polymers and other Materials, Proceedings of the ACS Symposium Series 391, American Chemical Society, Washington, DC, 1989.